Design of Practically Perfect-Reconstruction Cosine-Modulated Filter Banks: A Second-Order Cone Programming Approach

Wu-Sheng Lu[1], Tapio Saramäki[2], and Robert Bregović[2]

1. Dept. of Electrical and Computer Engineering,
   University of Victoria, Victoria, BC, Canada, V8W 3P6
   E-mail: wslu@ece.uvic.ca
2. Institute of Signal Processing, Tampere University of Technology
   P. O. Box 553, FIN-33101 Tampere, Finland
   E-mails: ts@cs.tut.fi and bregovic@cs.tut.fi

Abstract

Designing optimal perfect-reconstruction (PR) and near PR (NPR) cosine-modulated filter banks is essentially a constrained nonlinear minimization problem. This paper proposes two second-order-cone-programming based algorithms for designing NPR and practically PR cosine-modulated filter banks with improved performance relative to several established design methods.

I. INTRODUCTION

An M-channel, maximally decimated, cosine-modulated filter bank can be characterized by a single prototype filter (PF), whose efficient implementation can be readily substantiated through polyphase decomposition. In addition, optimal synthesis of a cosine-modulated multirate system can be carried out with considerably reduced complexity compared to that of a general M-channel system as the work in the former case is focused on designing the PF alone. These benefits, among other things, have rendered the cosine-modulated filter banks one of the most useful classes of multirate systems. The literature on the subject is abundant, see, for example, [1]–[28] and the related work cited therein. Of particular interest within this filter bank class are biorthogonal cosine-modulated (BCM) filter banks as they offer reduced system delay while maintaining the perfect reconstruction (PR) or near PR (NPR) property. Recent progress in the analysis and design of BCM filter banks have been reported by several authors, see, for example, [18]–[21], [23]–[26], and [28]. Available design techniques for BCM filter banks now include the quadratic-constrained least-squares (QCLS) method [23], [20], [6] that minimizes the stopband energy of the PF subject to the PR constraints expressed as quadratic equalities in terms of the coefficients of the PF; the factorization-based method [19], [24], [25] that yields a parameterized realization in which the PR property is always ensured while minimizing the stopband energy of the PF in an unconstrained optimization setting; and the sequential design method [28] that is carried out by first designing a filter bank with a small number of channels and a relatively short filter length and then gradually increasing the number of channels as well as the filter length using a technique initiated in [5]. In addition, quadratic-constrained-optimization based algorithms [10] and fast design through window function optimization [11][22] for orthogonal cosine-modulated (OCM) filter banks have been proposed.

In essence, the design of a cosine-modulated filter bank is a nonconvex constrained optimization problem that has multiple local minimums, and it is generally agreed that which of the above-mentioned methods would result in a better design depends largely on the choice of optimization procedure and the complexity of the problem [25]. The focus of this paper is primarily on developing two new optimization algorithms that are tailored to the time-domain formulation set forth in [23] so as to obtain improved designs relative to several existing methods. In the first algorithm, the design starts with an initial point that corresponds to the PF minimizing its stopband energy without the PR constraints. This initial point is then iteratively updated by minimizing the upper bound of a linearized error measure of the time-domain PR

constraints within a convex region defined by a constraint on the stopband energy of the PF. The optimization problem so formulated turns out to be a *second-order cone programming* (SOCP) problem [30]–[32] which can be solved using efficient interior-point algorithms in polynomial-time complexity [33], [34]. By controlling the PF's stopband energy, each iterate of the algorithm corresponds to an NPR filter bank whose PR distortion is reduced at the cost of increased stopband energy of the PF. In this way, for a given channel number and PF length, one is in a position to make best tradeoff between the PR distortions and the stopband energy of the PF (which is closely related to the performance of the analysis and synthesis filters). The second algorithm is aimed at direct minimization of the PF's stopband energy subject to the time-domain PR constraints. By parameterizing a linear approximation of the PR constraints and imposing a norm constraint on the increment vector of the design variables, it is shown that the optimization problem at hand can also be converted into an SOCP problem. As will be demonstrated by simulation results, the second algorithm can be used to design practically PR OCM and BCM filter banks with improved performance compared to several established design methods.

The paper is organized as follows. Section 2 provides a brief review of cosine-modulated filter banks and SOCP. Section 3 starts with an analysis of the time-domain PR constraints [23] and presents an SOCP formulation for the design of NPR BCM filter banks. The second SOCP-based algorithm for the design of PR OCM/BCM filter banks is described in Section 4, and several design examples are presented in Section 5.

Throughout the paper, boldfaced characters denote matrices and vectors; $\boldsymbol{I}$ denotes the identity matrix of an appropriate dimension and $\|\cdot\|$ denotes the standard Euclidean norm; $\boldsymbol{M} \succ \boldsymbol{0}$ and $\boldsymbol{M} \succeq \boldsymbol{0}$ denote that matrix $\boldsymbol{M}$ is positive definite and $\boldsymbol{M}$ is positive semidefinite, respectively.

II. Preliminaries

A. BCM filter banks

An M-channel, maximally decimated BCM filter bank is illustrated in Fig. 1, where the coefficients of the analysis and synthesis filters are given by

$$h_k(n) = 2h(n)\cos\left[\frac{\pi}{M}\left(k+\frac{1}{2}\right)\left(n-\frac{D}{2}\right)+(-1)^k\frac{\pi}{4}\right] \tag{1a}$$

and

$$f_k(n) = 2h(n)\cos\left[\frac{\pi}{M}\left(k+\frac{1}{2}\right)\left(n-\frac{D}{2}\right)-(-1)^k\frac{\pi}{4}\right] \tag{1b}$$

for $0 \leq k \leq M-1$ and $0 \leq n \leq N-1$, respectively, $\{h(n)\}$ is the impulse response of the finite-impulse-response (FIR) PF, and D denotes the system delay.

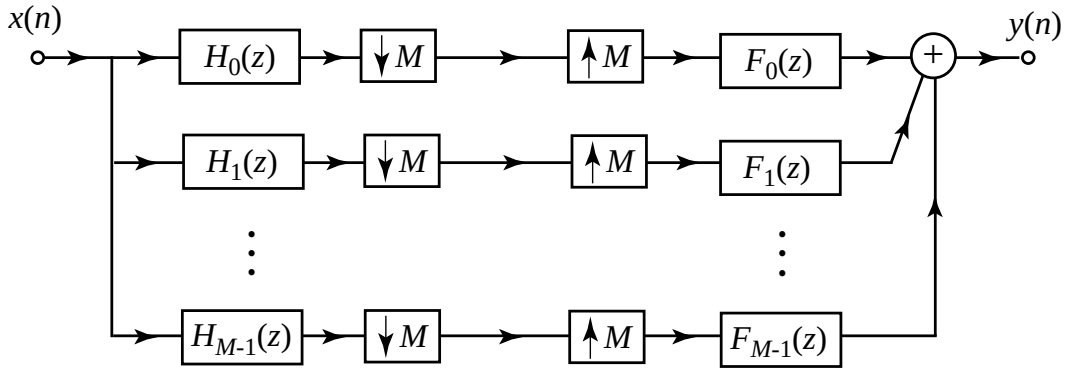

Fig. 1. M-channel maximally decimated filter bank

BCM filter bank structures other than that of (1) can also be generated using different DCT modulations [23]. In this paper, however, we concentrate on the DCT-IV BCM filter banks as specified by (1), along with the following assumptions: (i) the channel number M is even, (ii) the filter length N assumes the form $N = 2mM$ for some positive integer m, and (iii) the system delay assumes the form $D = 2Ms + d$ where $s \geq 0$ is an integer and $d = 2M - 1$. The rationale of these assumptions have been addressed in the literature [23], [25], [26]. In short, these assumptions are made for the sake of system performance rather than convenience. For example, if the value of d is specified other than $2M-1$, then some coefficients of the PF have to be zero [23] in order for the BCM filter bank to be PR, which will severely degrade the performance.

The input-output relation of the system in the z-domain is given by

$$Y(z) = T_0(z)X(z) + \sum_{l=1}^{M-1} T_l(z)X(ze^{-j2\pi l/M}) \tag{2a}$$

where

$$T_0(z) = \frac{1}{M}\sum_{k=0}^{M-1} F_k(z)H_k(z) \tag{2b}$$

is the distortion transfer function which determines the distortion caused by the system for the unaliased component $X(z)$, and

$$T_l(z) = \frac{1}{M}\sum_{k=0}^{M-1} F_k(z)H_k(ze^{-j2\pi l/M}) \qquad \text{for } l = 1,\ \ldots,\ M-1 \tag{2c}$$

are the alias transfer functions that determine how the aliased components $X(ze^{-j2\pi l/M})$ are

attenuated [8], [26]. It follows that the BCM filter bank holds the PR property if and only if

$$T_0(z) = z^{-D} \tag{3a}$$

and

$$T_l(z) = 0 \qquad \text{for } l = 1,\ \ldots,\ M-1 \tag{3b}$$

where D is the system delay. In such a case, (2a) becomes $Y(z) = z^{-D}X(z)$ which implies that $y(n) = x(n-D)$, i.e., the output is a delayed replica of the input.

There are two types of PR characterization. In the frequency domain, the PR conditions are characterized based on (3) as

$$T_0(e^{j\omega}) = e^{-jD\omega} \qquad \text{for } \omega \in [0,\ \pi] \tag{4a}$$

and

$$T_l(e^{j\omega}) = 0 \qquad \text{for } \omega \in [0,\ \pi] \text{ and } 1 \le l \le M-1 \tag{4b}$$

In the time-domain, the PR conditions can be described by the following set of quadratic equations [23]:

$$\boldsymbol{h}^T \boldsymbol{Q}_{l,n} \boldsymbol{h} = c_n \qquad \text{for } 0 \le n \le 2m-2 \text{ and } 0 \le l \le M-1 \tag{5a}$$

where $\boldsymbol{h} = [h_0 \ \ h_1 \ \ \cdots \ \ h_{N-1}]^T$ collects the coefficients of the PF, and

$$\boldsymbol{Q}_{l,n} = \boldsymbol{V}_{d-l}\boldsymbol{D}_n\boldsymbol{V}_l^T + \boldsymbol{V}_{d-M-l}\boldsymbol{D}_n\boldsymbol{V}_{M+l}^T \tag{5b}$$

$$\boldsymbol{D}_n(i,j) = \begin{cases} 1 & \text{if } i+j = n \\ 0 & \text{otherwise} \end{cases} \tag{5c}$$

$$\boldsymbol{V}_l(i,j) = \begin{cases} 1 & \text{if } i = l+2jM \\ 0 & \text{otherwise} \end{cases} \tag{5d}$$

$$c_n = \frac{1}{2M}\delta(n-s) \tag{5e}$$

for $i = 0, 1, \ldots, N-1$, and $j = 0, 1 \ldots, N-1$.

A filter bank that does not hold the PR property might still be useful if it is near PR (NPR). Typically the "closeness" of a biorthogonal filter bank to the PR property is measured in the frequency-domain by means of

(i) Amplitude distortion

$$e_m(\omega) = 1 - |T_0(e^{j\omega})| \qquad \text{for } \omega \in [0,\ \pi] \tag{6}$$

(ii) Group-delay distortion

$$e_{gd}(\omega) = D - \arg[T_0(e^{j\omega})] \qquad \text{for } \omega \in [0,\ \pi] \tag{7}$$

(iii) Worst-case aliasing error

$$e_a(\omega) = \max_{1\le l\le M-1} |T_l(e^{j\omega})| \qquad \text{for } \omega \in [0,\ \pi] \tag{8}$$

A filter bank is said to be NPR if its $e_m(\omega)$, $e_{gd}(\omega)$ and $e_a(\omega)$ are uniformly small in magnitude for $0 \le \omega \le \pi$.

Concerning the PF, it is often desirable to construct a PR or NPR BCM filter bank with the PF's stopband energy

$$e_2(\boldsymbol{h}) = \int_{\omega_s}^{\pi} |H(e^{j\omega})|^2\, d\omega \tag{9a}$$

minimized, where

$$H(e^{j\omega}) = \sum_{k=0}^{N-1} h_k e^{-jk\omega} \tag{9b}$$

is the frequency response of the PF, and

$$\omega_s = \frac{(1+\rho)\pi}{2M} \qquad \text{with } \rho > 0 \tag{9c}$$

is the stopband edge of the PF. An alternative of (9a) is the peak value of $|H(e^{j\omega})|$ over the stopband, i.e.,

$$e_\infty(\boldsymbol{h}) = \max_{\omega\in[\omega_s,\pi]} |H(e^{j\omega})| \tag{10}$$

B. Second-order cone programming

Second-order cone programming (SOCP), also known as conic quadratic programming [31], is a subclass of well-structured convex programming problems where a linear function is minimized subject to a set of second-order cone constraints and possibly a set of linear equality constraints:

$$\text{minimize} \quad \boldsymbol{c}^T\boldsymbol{x} \tag{11a}$$

$$\text{subject to:} \quad \|\boldsymbol{A}_i\boldsymbol{x} + \boldsymbol{b}_i\| \le \boldsymbol{c}_i^T\boldsymbol{x} + d_i \quad i = 1, 2, \ldots, K \tag{11b}$$

$$\mathbf{F}\boldsymbol{x} = \boldsymbol{g} \tag{11c}$$

where $\boldsymbol{c} \in \mathcal{R}^{n\times 1},\ \boldsymbol{A}_i \in \mathcal{R}^{(n_i-1)\times n},\ b_i \in \mathcal{R}^{(n_i-1)\times 1},\ c_i \in \mathcal{R}^{n\times 1}$, and $d_i \in \mathcal{R}$. The term "second-order cone" reflects the fact that each constraint in (11b) is equivalent to the following *conic* constraint:

$$\begin{bmatrix} \boldsymbol{c}_i^T \\ \boldsymbol{A}_i \end{bmatrix} \boldsymbol{x} + \begin{bmatrix} d_i \\ \boldsymbol{b}_i \end{bmatrix} \in \mathcal{C}_i$$

where $\mathcal{C}_i$ is the second-order cone in $\mathcal{R}^{n_i}$:

$$\mathcal{C}_i = \left\{ \begin{bmatrix} t \\ \boldsymbol{u} \end{bmatrix} : \ \boldsymbol{u} \in \mathcal{R}^{(n_i-1)\times 1},\ t \geq 0,\ \|\boldsymbol{u}\| \leq t \right\} \tag{12}$$

Fig. 2 illustrates the second-order cone in space $\mathcal{R}^3$.

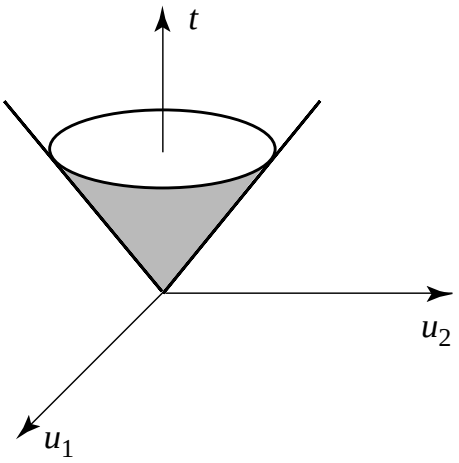

Fig. 2. The second-order cone in $\mathcal{R}^3$.

From (11), it is evident that SOCP includes linear programming and convex quadratic programming as special cases. On the other hand, SOCP itself is a subclass of semidefinite programming (SDP) [30], [31], [35] because each constraint in (11b) can be expressed as the linear matrix inequality

$$\begin{bmatrix} (\boldsymbol{c}_i^T\boldsymbol{x} + d_i)\boldsymbol{I} & \boldsymbol{A}_i\boldsymbol{x} + \boldsymbol{b}_i \\ (\boldsymbol{A}_i\boldsymbol{x} + \boldsymbol{b}_i)^T & \boldsymbol{c}_i^T\boldsymbol{x} + d_i \end{bmatrix} \succeq \boldsymbol{0}$$

Software that implement various polynomial-time interior-point optimization algorithms for SOCP and SDP are available [33], [34], [36]. It is important to stress, however, that in general the problem in (11) can be solved more efficiently using an SOCP solver provided, for example, by SeDuMi [33] and SDPT3 [34] than solving it in an equivalent SDP setting [30].

III. An SOCP Formulation for NPR Filter Banks

A. Remarks on the time-domain PR constraints in (5)

The constraints in (5) are second-order equalities, each defining a nonconvex set in space $\mathcal{R}^N$. The feasible region, defined as a set in $\mathcal{R}^N$ characterizing all M-channel PR BCM filter banks of length N, is the intersection of these nonconvex sets, which is in general nonconvex. For illustration purposes, let us consider a simple case with $M = 2$, $m = 2$, $s = 0$, and $d = 3$. According to (5a), there are the following six constraints which can be specified using (5b)–(5e)

as

$$\boldsymbol{h}^T\boldsymbol{Q}_{0,0}\boldsymbol{h} = h_0h_3 + h_1h_2 = \frac{1}{4} \tag{13a}$$

$$\boldsymbol{h}^T\boldsymbol{Q}_{0,1}\boldsymbol{h} = h_0h_7 + h_2h_5 + h_3h_4 + h_1h_6 = 0 \tag{13b}$$

$$\boldsymbol{h}^T\boldsymbol{Q}_{0,2}\boldsymbol{h} = h_4h_7 + h_5h_6 = 0 \tag{13c}$$

$$\boldsymbol{h}^T\boldsymbol{Q}_{1,0}\boldsymbol{h} = h_1h_2 + h_0h_3 = \frac{1}{4} \tag{13d}$$

$$\boldsymbol{h}^T\boldsymbol{Q}_{1,1}\boldsymbol{h} = h_1h_6 + h_3h_4 + h_2h_5 + h_0h_7 = 0 \tag{13e}$$

$$\boldsymbol{h}^T\boldsymbol{Q}_{1,2}\boldsymbol{h} = h_5h_6 + h_4h_7 = 0 \tag{13f}$$

Obviously, the constraints in (13d)–(13f) are redundant and, hence, the PR conditions are in this case reduced to (13a)–(13c). The redundancy exhibited in the above example is not just an incident. As matter of fact, with $d = 2M - 1$ (as we shall assume in this paper) it can be verified that all non-redundant constraints in (5a) are given by

$$a_{l,n}(\boldsymbol{h}) = \boldsymbol{h}^T\boldsymbol{Q}_{l,n}\boldsymbol{h} - c_n = 0 \qquad \text{for } 0 \le n \le 2m-2 \text{ and } 0 \le l \le M/2-1 \tag{14}$$

thereby reducing the total number of constraints from $M(2m-1)$ to $M(2m-1)/2 = (N - M)/2$. Since there are N coefficients in the PF, the "degrees of freedom" in the design is $N - (N - M)/2 = (N + M)/2$ that is proportional to both the channel number and filter length. Consequently, for a given channel number M (thus fixed stopband, see (9c)), improved designs are expected as the filter length increases.

As an additional remark, note that in the above example we have assigned the value of d to $d = 2M - 1 = 3$. To see the effect of having a different value for d, let $d = 2$ which leads the six constraints in (5a) (here we are dealing with a case with $d \neq 2M - 1$ and the constraints in (5a) are in general not redundant):

$$\boldsymbol{h}^T\boldsymbol{Q}_{0,0}\boldsymbol{h} = 2h_0h_2 = \frac{1}{4} \tag{15a}$$

$$\boldsymbol{h}^T\boldsymbol{Q}_{0,1}\boldsymbol{h} = 2(h_0h_6 + h_2h_4) = 0 \tag{15b}$$

$$\boldsymbol{h}^T\boldsymbol{Q}_{0,2}\boldsymbol{h} = 2h_4h_6 = 0 \tag{15c}$$

$$\boldsymbol{h}^T\boldsymbol{Q}_{1,0}\boldsymbol{h} = h_1^2 = \frac{1}{4} \tag{15d}$$

$$\boldsymbol{h}^T\boldsymbol{Q}_{1,1}\boldsymbol{h} = h_3^2 + 2h_1h_5 = 0 \tag{15e}$$

$$\boldsymbol{h}^T\boldsymbol{Q}_{1,2}\boldsymbol{h} = h_5^2 + 2h_3h_7 = 0 \tag{15f}$$

Equation (15a) implies that both h_0 and h_2 are nonzero, which in conjunction with (15b) and (15c) leads to $h_4 = 0$ and $h_6 = 0$. In addition, (15d) implies that h_1 is forced to be either 0.5 or

-0.5. With $h_1,\ h_4,$ and h_6 fixed and three remaining constraints in (15a), (15e), and (15f), it is rather difficult for the PF of length 8 to generate a good BCM filter bank. This explains why the use of d less than $2M-1$ is not preferred.

In the rest of this paper, $d = 2M-1$ is always assumed, which leads (5b) to

$$Q_{l,n} = \boldsymbol{V}_{2M-l-1}\boldsymbol{D}_n\boldsymbol{V}_l^T + \boldsymbol{V}_{M-l-1}\boldsymbol{D}_n\boldsymbol{V}_{M+l}^T \tag{16}$$

and we shall use (14) and (16), instead of (5a) and (5b), as the PR constraints for BCM filter banks.

When the PF has a linear phase response, the system delay of the filter bank is $D = N-1$ where N is the length of the PF, and the impulse responses of the synthesis filters become $f_k(n) = h_k(N-n-1)$ for $0 \le k \le M-1$ and the filter bank in this case is said to be orthogonal [26]. The design variables in this case are the components in the first half of the PF's impulse response, i.e., $\boldsymbol{h} = [h_0 \ \ h_1 \ \ \cdots h_{mM-1}]^T$, and the time-domain PR constraints become [15]

$$a_{l,n}(\boldsymbol{h}) = \boldsymbol{h}^T\boldsymbol{Q}_{l,n}\boldsymbol{h} - c_n = 0 \qquad \text{for } 0 \le n \le m-1,\ 0 \le l \le M/2-1 \tag{17a}$$

where

$$\boldsymbol{Q}_{l,n} = \boldsymbol{V}_l\boldsymbol{J}\boldsymbol{D}_n\boldsymbol{V}_l^T + \boldsymbol{V}_{M+l}\boldsymbol{J}\boldsymbol{D}_n\boldsymbol{V}_{M+l}^T \tag{17b}$$

and $\boldsymbol{D}_n,\ \boldsymbol{V}_l,$ and c_n are defined in (5c)–(5e). It follows that there is a total of $mM/2$ PR constraints, hence the degrees of freedom in the design of OCM filter banks is $N/2 - mM/2 = N/4$.

B. Stopband energy of the prototype filter

The frequency response of the PF can be expressed as

$$H(e^{j\omega}) = \sum_{k=0}^{N-1} h_k e^{-jk\omega} = \boldsymbol{h}^T\boldsymbol{p}(\omega)$$

with $\boldsymbol{p}(\omega) = [1 \ \ e^{-j\omega} \ \ \cdots \ \ e^{-j(N-1)\omega}]^T$. Using (17), the stopband energy becomes

$$e_2(\boldsymbol{h}) = \int_{\omega_s}^{\pi} \boldsymbol{h}^T\boldsymbol{L}(\omega)\boldsymbol{h}\, d\omega$$

where for each fixed ω, $\boldsymbol{L}(\omega)$ is a symmetric, positive-semidefinite Toeplitz matrix [37] determined by its first row $[1 \ \ \cos\omega \ \ \cos 2\omega \ \ \cdots \ \ \cos(N-1)\omega]$. Therefore, we have

$$e_2(\boldsymbol{h}) = \boldsymbol{h}^T\boldsymbol{P}\boldsymbol{h} \tag{18}$$

where

$$\boldsymbol{P} = \int_{\omega_s}^{\pi} \boldsymbol{L}(\omega)\, d\omega$$

is a symmetric positive-definite Toeplitz matrix determined by its first row $[\pi - \omega_s \quad -\sin\omega_s \quad -\sin 2\omega_s/2 \quad \cdots \quad -\sin(N-1)\omega_s/(N-1)]$. The positive definiteness of matrix $\boldsymbol{P}$ in (18) implies that function $e_2(\boldsymbol{h})$ is globally convex in the entire space $\mathcal{R}^N$ [38], which turns out to be instrumental in the subsequent development.

C. The underlying idea: An intuitive description

The design of BCM filter banks can be stated in the time-domain as follows [23]:

$$\text{minimize} \quad e_2(\boldsymbol{h}) = \boldsymbol{h}^T \boldsymbol{P} \boldsymbol{h} \tag{19a}$$

$$\text{subject to:} \quad \text{constraints in (14)} \tag{19b}$$

A difference between the above formulation and the one in [23] is that the number of the constraints involved in (19b) is only a half of that in Eq. (65) of [23].

Suppose we start with an initial design that minimizes the stopband energy $e_2(\boldsymbol{h})$ in (19a) *without* the PR constraints in (19b) but impose a coefficient normalization condition (to avoid the trivial zero solution):

$$\text{minimize} \quad e_2(\boldsymbol{h}) = \boldsymbol{h}^T \boldsymbol{P} \boldsymbol{h} \tag{20a}$$

$$\text{subject to:} \quad \sum_{i=0}^{N-1} h_i = 1 \tag{20b}$$

and denote the solution of (20) by $\boldsymbol{h}_0$. Because of the freedom from the PR constraints, the value $e_2(\boldsymbol{h}_0)$ is considerably smaller than what a PR prototype filter can achieve. If we define a contour of $e_2(\boldsymbol{h})$ at level value c as

$$\mathcal{S}_c = \{\boldsymbol{h} : e_2(\boldsymbol{h}) = c\} \tag{21}$$

then point $\boldsymbol{h}_0$ lies on the contour $\mathcal{S}_{c_0}$ with $c_0 = e_2(\boldsymbol{h}_0)$ and the global convexity of function $e_2(\boldsymbol{h})$ implies that (i) the entire feasible region $\mathcal{F} = \{\boldsymbol{h} : \boldsymbol{h}$ satisfies all constraints in (14)$\}$ lies outside region $\mathcal{A}_{c_0}$ which is the region enclosed with contour $\mathcal{S}_{c_0}$ (see Fig. 3), and (ii) as the level value c grows, the family of contours $\{\mathcal{S}_c\}$ grows accordingly and will eventually meet and then intersect with $\mathcal{F}$, see Fig. 3 for an illustration.

Because of the nonconvexity of $\mathcal{F}$, multiple minimizers likely exist (in Fig. 3, there are two minimizers: a global minimizer $\boldsymbol{h}^*$ and a local minimizer $\tilde{\boldsymbol{h}}$). From Fig. 3, it is intuitively

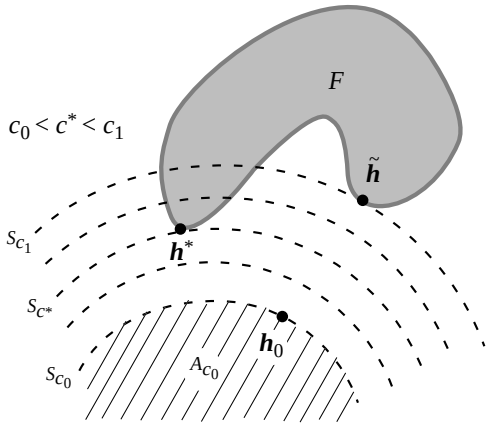

Fig. 3. A growing family of contours for the objective function $e_2(\boldsymbol{h})$ meets the nonconvex feasible region $\mathcal{F}$, and a global minimizer $\boldsymbol{h}^*$ and a local minimizer $\tilde{\boldsymbol{h}}$ are identified.

clear that if one lets the contours grow from $\mathcal{S}_{c_0}$ *gradually in small steps*, then the family of contours will meet the global minimizer $\boldsymbol{h}^*$ first. This idea of approaching the global minimizer can be substantiated in the context of optimization as follows. First, we define an appropriate measure of closeness of the PF to the PR property. A convenient least-squares measure can be constructed based on the PR constraints in (14) as follows:

$$f(\boldsymbol{h}) = \sum_{l=0}^{\frac{M}{2}-1} \sum_{n=0}^{2m-2} (\boldsymbol{h}^T \boldsymbol{Q}_{l,n} \boldsymbol{h} - c_n)^2 \tag{22}$$

Because $f(\boldsymbol{h}) = 0$ if and only if $\boldsymbol{h} \in \mathcal{F}$, a point $\boldsymbol{h}$ with a smaller $f(\boldsymbol{h})$ is regarded as "closer" to $\mathcal{F}$. Now consider a scenario where point $\boldsymbol{h}_0$ is updated to $\boldsymbol{h}_1$ by minimizing $f(\boldsymbol{h})$ within the region bounded by a contour $\mathcal{S}_c$ with c moderately larger than c_0. The situation is illustrated in Fig. 4, where the shaded region $\mathcal{A}_c = \{\boldsymbol{h} : e_2(\boldsymbol{h}) \leq c\}$ is convex with $\mathcal{S}_c$ as its boundary and the minimization process is indicated with a dashed curve connecting points $\boldsymbol{h}_0$ and $\boldsymbol{h}_1$.

Once point $\boldsymbol{h}_1$ is obtained, the frontier of region $\mathcal{A}_c$ further advances towards $\mathcal{F}$ by modifying its boundary $\mathcal{S}_c$ with a slightly increased c. Within the enlarged region, point $\boldsymbol{h}_1$ is updated to a new point $\boldsymbol{h}_2$ in a similar manner. In analytical terms, in the kth iteration of the process, point $\boldsymbol{h}_k$ is updated to $\boldsymbol{h}_{k+1} = \boldsymbol{h}_k + \boldsymbol{\delta}$ where $\boldsymbol{\delta}$ solves the constrained optimization problem

$$\underset{\boldsymbol{\delta}}{\text{minimize}} \quad f(\boldsymbol{h}_k + \boldsymbol{\delta}) \tag{23a}$$

$$\text{subject to:} \quad e_2(\boldsymbol{h}_k + \boldsymbol{\delta}) \leq c \tag{23b}$$

with c a constant whose value gradually (and monotonically) increases as the iteration continues. The above process is terminated when the minimized value $f(\boldsymbol{h}_{k+1})$ falls below a prescribed threshold, and the point $\boldsymbol{h}_{k+1}$ is then taken as the impulse response of the PF of an NPR

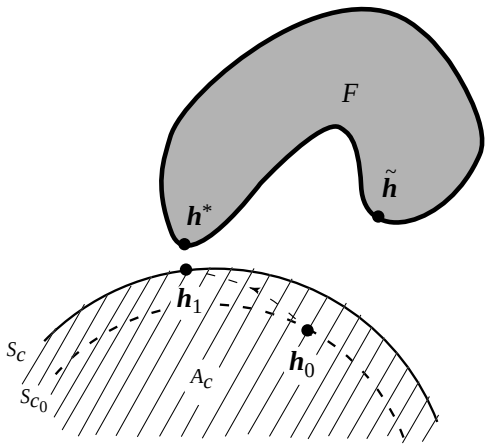

Fig. 4. Point $\boldsymbol{h}_0$ is updated to $\boldsymbol{h}_1$ within the convex region $\mathcal{A}_c$ by minimizing the PR error measure $f(\boldsymbol{h})$ in (22). The dashed curve connecting the two points is a typical trajectory when an SOCP is applied.

BCM filter bank. In what follows, we develop an SOCP formulation for the problem in (23).

D. An iterative SOCP formulation

The function $f(\boldsymbol{h})$ in (22) is a smooth, fourth-order function of $\boldsymbol{h}$ with its Hessian given by

$$\nabla^2 f(\boldsymbol{h}) = 8\sum_l \sum_n \boldsymbol{Q}_{l,n}(\boldsymbol{h}\boldsymbol{h}^T)\boldsymbol{Q}_{l,n}^T + 2\sum_l \sum_n (\boldsymbol{h}^T\boldsymbol{Q}_{l,n}\boldsymbol{h} - c_n)(\boldsymbol{Q}_{l,n} + \boldsymbol{Q}_{l,n}^T) \tag{24}$$

The first term in (24) is positive definite but the second term is not. Hence $f(\boldsymbol{h})$ is in general not a convex function. However, when point $\boldsymbol{h}$ is sufficiently close to region $\mathcal{F}$, terms $\boldsymbol{h}^T\boldsymbol{Q}_{l,n}\boldsymbol{h} - c_n$ become near zero and the first term in (24) dominates $\nabla^2 f(\boldsymbol{h})$. Consequently, as $\boldsymbol{h}$ is near region $\mathcal{F}$, $f(\boldsymbol{h})$ behaves like a convex function. A linear approximation of $f(\boldsymbol{h})$ in the vicinity of $\boldsymbol{h}_k$ is given by

$$f(\boldsymbol{h}_k + \boldsymbol{\delta}) \approx f(\boldsymbol{h}_k) + \boldsymbol{g}_k^T\boldsymbol{\delta} \tag{25a}$$

where $\boldsymbol{g}_k$ is the gradient of $f(\boldsymbol{h})$ at $\boldsymbol{h}_k$ that can be evaluated as

$$\boldsymbol{g}_k = 4\sum_{l=0}^{\frac{M}{2}-1} \sum_{n=0}^{2m-2} (\boldsymbol{h}_k^T\boldsymbol{Q}_{l,n}\boldsymbol{h}_k - c_n)\boldsymbol{Q}_{l,n}\boldsymbol{h}_k \tag{25b}$$

Note that the approximation in (25a) is valid provided that

$$\|\boldsymbol{\delta}\| \text{ is small} \tag{25c}$$

Under these circumstances, the problem in (23) can be converted into the following form:

$$\text{minimize} \quad \eta \tag{26a}$$

$$\text{subject to:} \quad |f(\boldsymbol{h}_k) + \boldsymbol{g}_k^T\boldsymbol{\delta}| \le \eta \tag{26b}$$

$$\|\boldsymbol{\delta}\| \leq \beta_1 \tag{26c}$$

$$e_2(\boldsymbol{h}_k + \boldsymbol{\delta}) \leq c \tag{26d}$$

where η is the absolute bound of the linearized PR error function, which can be treated as an auxiliary variable, and β_1 is a small positive scalar.

Defining

$$\boldsymbol{x} = \begin{bmatrix} \eta \\ \boldsymbol{\delta} \end{bmatrix} \qquad \text{and} \qquad \boldsymbol{c} = \begin{bmatrix} 1 \\ 0 \\ \vdots \\ 0 \end{bmatrix} \tag{27}$$

the objective function in (26a) can be expressed as $\boldsymbol{c}^T\boldsymbol{x}$. Next, we write the constraint in (26b) as the following two one-side linear inequalities:

$$f(\boldsymbol{h}_k) + \boldsymbol{g}_k^T\boldsymbol{\delta} \;\; \leq \;\; \eta$$

and

$$-f(\boldsymbol{h}_k) - \boldsymbol{g}_k^T\boldsymbol{\delta} \;\; \leq \;\; \eta$$

which lead to

$$\boldsymbol{G}_k\boldsymbol{x} \;\; \leq \;\; \boldsymbol{d}_k$$

with

$$\boldsymbol{G}_k = \begin{bmatrix} -1 & \boldsymbol{g}_k^T \\ -1 & -\boldsymbol{g}_k^T \end{bmatrix} \qquad \text{and} \qquad \boldsymbol{d}_k = \begin{bmatrix} -f(\boldsymbol{h}_k) \\ f(\boldsymbol{h}_k) \end{bmatrix} \tag{28}$$

The norm constraint in (26c) can be expressed as

$$\|\tilde{\boldsymbol{I}}\boldsymbol{x}\| \leq \beta_1$$

where $\tilde{\boldsymbol{I}} = [\boldsymbol{0} \;\; \boldsymbol{I}]$. Based on (18), the constraint in (26d) can be written as

$$\|\tilde{\boldsymbol{P}}\boldsymbol{x} + \tilde{\boldsymbol{b}}_k\| \leq \beta_2 \tag{29}$$

where

$$\tilde{\boldsymbol{P}} = [\boldsymbol{0} \;\; \boldsymbol{P}^{1/2}],\; \tilde{\boldsymbol{b}}_k = \boldsymbol{P}^{1/2}\boldsymbol{h}_k,\; \beta_2 = c^{1/2} \tag{30}$$

and $\boldsymbol{P}^{1/2}$ denotes the symmetric square root of matrix $\boldsymbol{P}$. Problem (26) now becomes

$$\text{minimize} \quad \boldsymbol{c}^T\boldsymbol{x} \tag{31a}$$

$$\text{subject to:} \quad \boldsymbol{G}_k\boldsymbol{x} \leq \boldsymbol{d}_k \tag{31b}$$

$$\|\tilde{\boldsymbol{I}}x\| \leq \beta_1 \tag{31c}$$

$$\|\tilde{\boldsymbol{P}}\boldsymbol{x} + \tilde{\boldsymbol{b}}_k\| \leq \beta_2 \tag{31d}$$

which is obviously an SOCP problem (see (11)). The above problem involves $N+1$ variables, two linear inequality constraints, and two conic constraints.

E. A summary of the design method

The proposed design method, which is aimed at a satisfactory NPR BCM filter bank, can now be summarized as follows.

It consists of an outer loop and an inner loop of iterations. The outer loop is to

(i) determine whether or not the optimization process should continue and, if yes,

(ii) provide the inner loop with an "initial point" $\boldsymbol{h}_0$ and the values of bounds β_1 and β_2,

while the inner loop consists of

(i) start with an $\boldsymbol{h}_0$ provided by the outer loop and set counter $k=0$ and a tolerance ε;

(ii) use (28) and (30) to evaluate $\boldsymbol{G}_k,\ \boldsymbol{d}_k,$ and $\tilde{\boldsymbol{b}}_k$;

(iii) apply an SOCP solver to problem (31) for the optimal $\boldsymbol{x}_k$;

(iv) obtain $\boldsymbol{\delta}_k = \boldsymbol{x}_k(2:N+1)$ and update $\boldsymbol{h}_k$ to $\boldsymbol{h}_{k+1} = \boldsymbol{h}_k + \boldsymbol{\delta}_k$;

(v) examine a convergence criterion such as $\|\boldsymbol{\delta}_k\| < \varepsilon$ (or $e_2(\boldsymbol{h}_k) - e_2(\boldsymbol{h}_{k+1}) < \varepsilon$, or the number of iterations exceeds a given bound K); if yes, terminate the inner loop and go back to the outer loop with $\boldsymbol{h}_{k+1}$ as the new initial point in the next round of inner-loop iterations, otherwise set $k := k+1$ and repeat from step (ii).

A flowchart that explains the interplay between the two loops is shown in Fig. 5.

F. The first initial point $\boldsymbol{h}_0$

The initial point for the inner-loop is provided by the output of the preceding round of inner-loop iterations except the very first $\boldsymbol{h}_0$ which cannot be provided by the inner loop. This $\boldsymbol{h}_0$ can be obtained by solving problem (20). We first parameterize *all* vectors $\boldsymbol{h}$ satisfying constraint (20b) as

$$\boldsymbol{h} = \boldsymbol{u}_N + \hat{\boldsymbol{I}}\boldsymbol{\xi} \tag{32}$$

where

$$\boldsymbol{u}_N = \begin{bmatrix} 0 \\ \vdots \\ 0 \\ 1 \end{bmatrix}, \quad \hat{\boldsymbol{I}} = \begin{bmatrix} 1 & & & 0 \\ & \ddots & \mathbf{0} & \vdots \\ & \mathbf{0} & 1 & 0 \\ -1 & \cdots & -1 & -1 \end{bmatrix}_{N\times(N-1)}$$

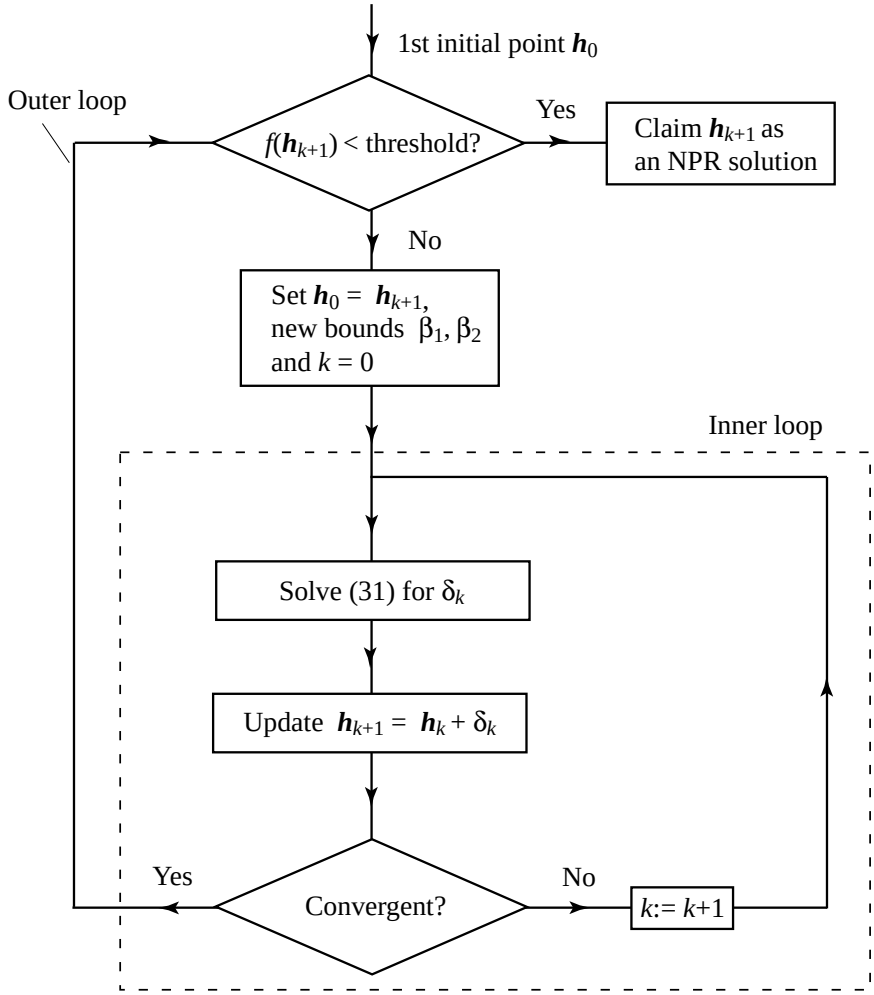

Fig. 5. A flowchart to illustrate how the two loops operate.

and $\boldsymbol{\xi}$ is an $(N-1)$-dimensional parameter vector. By substituting (32) into (20a), problem (20) is converted into the unconstrained problem

$$\underset{\boldsymbol{\xi}}{\text{minimize}}(\boldsymbol{u}_N + \hat{\boldsymbol{I}}\boldsymbol{\xi})^T \boldsymbol{P}(\boldsymbol{u}_N + \hat{\boldsymbol{I}}\boldsymbol{\xi})$$

which has a unique global minimizer

$$\boldsymbol{\xi}^* = -(\hat{\boldsymbol{I}}^T \boldsymbol{P}\hat{\boldsymbol{I}})^{-1}\hat{\boldsymbol{I}}^T \boldsymbol{P}\boldsymbol{u}_N$$

Using (32), the solution of problem (20) is obtained as

$$\boldsymbol{h}_0 = [\boldsymbol{I} - (\hat{\boldsymbol{I}}^T \boldsymbol{P}\hat{\boldsymbol{I}})^{-1}\hat{\boldsymbol{I}}^T \boldsymbol{P}]\boldsymbol{u}_N \tag{33}$$

which is merely the last column of matrix $\boldsymbol{I} - (\hat{\boldsymbol{I}}\boldsymbol{P}\hat{\boldsymbol{I}})^{-1}\hat{\boldsymbol{I}}^T \boldsymbol{P}$.

Although the PF associated with $\boldsymbol{h}_0$ in (33) has the least stopband energy, by minimizing $e_2(\boldsymbol{h})$ in (18) the PF's behavior over the passband is not under control and, more importantly, the

low group-delay requirement of the design cannot be easily taken into account. An alternative that alleviates these problems can be obtained by minimizing the weighted last-squares objective function

$$e_2(\boldsymbol{h}, w) = (1-w)\int_0^{\omega_p} |H(e^{j\omega}) - e^{-j\hat{D}\omega}|^2 d\omega + w\int_{\omega_a}^{\pi} |H(e^{j\omega})|^2 d\omega \tag{34}$$

where passband edge ω_p and stopband edge ω_a are related to ω_s as given by (9b) in a manner to be described later, $w \in (0,\ 1)$ is a scalar weight, $\hat{D} = D/2$, and D is the system's group delay. This quadratic function $e_2(\boldsymbol{h}, w)$ can be expressed in terms of $\boldsymbol{h}$ as

$$e_2(\boldsymbol{h}, w) = \boldsymbol{h}^T\boldsymbol{Q}\boldsymbol{h} - 2\boldsymbol{h}^T\boldsymbol{p} + q$$

where

$$\boldsymbol{Q} = (1-w)\boldsymbol{L}(\boldsymbol{v}_1) + w\boldsymbol{L}(\boldsymbol{v}_2)$$

$$\boldsymbol{p} = (1-\alpha)\begin{bmatrix} \sin\hat{D}\omega_p/\hat{D} \\ \sin(\hat{D}-1)\omega_p/(\hat{D}-1) \\ \vdots \\ \sin(\hat{D}-N+1)\omega_p/(\hat{D}-N+1) \end{bmatrix}$$

$$\boldsymbol{v}_1 = \begin{bmatrix} \omega_p \\ \sin\omega_p \\ \vdots \\ \sin(N-1)\omega_p/N-1 \end{bmatrix}$$

$$\boldsymbol{v}_2 = \begin{bmatrix} \pi-\omega_a \\ -\sin\omega_a \\ \vdots \\ \sin(N-1)\omega_a/N-1 \end{bmatrix}$$

$\boldsymbol{L}(\boldsymbol{v}_1)$ and $\boldsymbol{L}(\boldsymbol{v}_2)$ are symmetric and positive-definite Toeplitz matrices whose first columns are $\boldsymbol{v}_1$ and $\boldsymbol{v}_2$, respectively. The initial point $\boldsymbol{h}_0$ can be chosen as the unique global minimizer of $e_2(\boldsymbol{h}, w)$ and is given by

$$\boldsymbol{h}_0 = \boldsymbol{Q}^{-1}\boldsymbol{p} \tag{35}$$

Since the stopband energy is one of our primary concerns, the value of weight w is usually taken to be very close to one. In our computer simulations, it was found that the choices $\omega_p = 0.5\omega_s$ and $\omega_a = 0.9\omega_s$ work quite well.

G. Design of OCM filter banks

The algorithm described above can be used for the design of OCM filter banks with straightforward modifications. Since the PR constraints in this case are characterized by (17), the objective function in (22) needs to be modified to

$$f(\boldsymbol{h}) = \sum_{l=0}^{\frac{M}{2}-1} \sum_{n=0}^{m-1} (\boldsymbol{h}^T \boldsymbol{Q}_{l,n} \boldsymbol{h} - c_n) \tag{36}$$

where $\boldsymbol{Q}_{l,n}$ is defined by (17b) and $\boldsymbol{h} = [h_0 \;\; h_1 \;\; \cdots \;\; h_{mN-1}]^T$. In addition, the stopband energy in (18) becomes

$$e_2(\boldsymbol{h}) = 4\boldsymbol{h}^T \boldsymbol{P}_L \boldsymbol{h} \tag{37a}$$

where

$$\boldsymbol{P}_L = \int_{\omega_s}^{\pi} \boldsymbol{c}(\omega) \boldsymbol{c}^T(\omega)\, d\omega \tag{37b}$$

$$\boldsymbol{c}(\omega) = \left[\cos\left(\frac{N-1}{2}\right)\omega \;\; \cos\left(\frac{N-3}{2}\right)\omega \;\; \cdots \;\; \cos\left(\frac{\omega}{2}\right)\right]^T \tag{37c}$$

IV. An SOCP formulation for Practically PR Filter Banks

The best the SOCP-based algorithm proposed in Sec. 3 can offer is a satisfactory NPR filter bank, but not a PR filter bank (see Remark (2) in Sec. 4.E). In this section, we describe a different algorithm that directly minimizes the stopband energy of the PF subject to the PR constraints.

A. Parameterization of approximated PR constraints

Suppose we are in the kth iteration and seek an increment vector $\boldsymbol{\delta}$ to update $\boldsymbol{h}_k$ to $\boldsymbol{h}_{k+1} = \boldsymbol{h}_k + \boldsymbol{\delta}$ such that the PR constraints in (14) are better satisfied. For $\boldsymbol{\delta}$ with $\|\boldsymbol{\delta}\|$ small, the PR constraints can be approximated linearly and the requirement becomes

$$a_{l,n}(\boldsymbol{h}_k + \boldsymbol{\delta}) \approx a_{l,n}(\boldsymbol{h}_k) + \boldsymbol{g}_{l,n}^T \boldsymbol{\delta} = 0 \qquad \text{for } 0 \le n \le 2m-2 \text{ and } 0 \le l \le M/2-1 \tag{38}$$

where $\boldsymbol{g}_{l,n} = 2\boldsymbol{Q}_{l,n}\boldsymbol{h}_k$ is the gradient of $a_{l,n}(\boldsymbol{h})$ at $\boldsymbol{h}_k$. The system of linear equations in (38) can be written as

$$\boldsymbol{G}_k \boldsymbol{\delta} = -\boldsymbol{a}_k \tag{39}$$

where $\boldsymbol{G}_k \in R^{(N-M)/2 \times N}$ collects the $(N-M)/2$ rows $\boldsymbol{g}_{l,n}^T$ and $\boldsymbol{a}_k \in R^{(N-M)/2}$ consists of components $a_{l,n}(\boldsymbol{h}_k)$. It is well known that all solutions of the underdetermined linear system

(39) can be parameterized as

$$\boldsymbol{\delta} = \boldsymbol{V}_e\boldsymbol{\phi} + \boldsymbol{\delta}_s \tag{40}$$

where $\boldsymbol{\delta}_s = -\boldsymbol{G}_k^{\dagger}\boldsymbol{a}_k$ is a special solution of (39), $\boldsymbol{V}_e \in R^{N\times(N+M)/2}$ is matrix composed of $(N+M)/2$ basis column vectors of the null space of $\boldsymbol{G}_k$, and $\boldsymbol{\phi} \in \mathcal{R}^{(N+M)/2}$ is a parameter vector. A numerically reliable way to compute matrix $\boldsymbol{V}_e$ in (40) is through the singular-value decomposition [37] of $\boldsymbol{G}_k$, i.e., $\boldsymbol{G}_k = \boldsymbol{U}\boldsymbol{\Sigma}\boldsymbol{V}^T$ from which $\boldsymbol{V}_e$ is formed by the last $(N+M)/2$ columns of $\boldsymbol{V}$.

B. An iterative SOCP formulation

The stopband energy of the PF in the kth iteration can be expressed as

$$e(\boldsymbol{h}_k + \boldsymbol{\delta}) = (\boldsymbol{h}_k + \boldsymbol{\delta})^T\boldsymbol{P}(\boldsymbol{h}_k + \boldsymbol{\delta}) = \|\boldsymbol{P}^{\frac{1}{2}}(\boldsymbol{h}_k + \boldsymbol{\delta})\|^2$$

For $\boldsymbol{\delta}$ approximating the PR constraints, we use (40) to rewrite the stopband energy at $\boldsymbol{h}_k + \boldsymbol{\delta}$ as

$$e(\boldsymbol{h}_k + \boldsymbol{\delta}) = \|\boldsymbol{P}^{\frac{1}{2}}\boldsymbol{V}_e\boldsymbol{\phi} + \boldsymbol{b}_k\|^2 \tag{41}$$

where $\boldsymbol{b}_k = \boldsymbol{P}^{\frac{1}{2}}(\boldsymbol{h}_k + \boldsymbol{\delta}_s)$. The optimization problem in (19) can now be converted to

$$\begin{aligned} \text{minimize} \quad & \eta && \text{(42a)}\\ \text{subject to:} \quad & \|\boldsymbol{P}^{\frac{1}{2}}\boldsymbol{V}_e\boldsymbol{\phi} + \boldsymbol{b}_k\| \le \eta && \text{(42b)}\\ & \|\boldsymbol{V}_e\boldsymbol{\phi} + \boldsymbol{\delta}_s\| \le \beta && \text{(42c)} \end{aligned}$$

where β is a small positive scalar to control the magnitude of $\boldsymbol{\delta}$ in (40). If we let $\boldsymbol{x} = [\eta \;\; \boldsymbol{\delta}^T]^T$, $\boldsymbol{c} = [1 \;\; 0 \;\cdots 0]^T$, $\tilde{\boldsymbol{P}} = [\boldsymbol{0} \;\; \boldsymbol{P}^{1/2}\boldsymbol{V}_e]$, and $\tilde{\boldsymbol{V}}_e = [\boldsymbol{0} \;\; \boldsymbol{V}_e]$, then problem (42) can be expressed as

$$\begin{aligned} \text{minimize} \quad & \boldsymbol{c}^T\boldsymbol{x} && \text{(43a)}\\ \text{subject to:} \quad & \|\tilde{\boldsymbol{P}}\boldsymbol{x} + \boldsymbol{b}_k\| \le \boldsymbol{c}^T\boldsymbol{x} && \text{(43b)}\\ & \|\tilde{\boldsymbol{V}}_e\boldsymbol{x} + \boldsymbol{\delta}_s\| \le \beta && \text{(43c)} \end{aligned}$$

which is obviously an SOCP problem. Solving (43), vector $\boldsymbol{\phi}$ is obtained as the last $(N+M)/2$ components of solution $\boldsymbol{x}$ and vector $\boldsymbol{\delta}$ is calculated using (40). Point $\boldsymbol{h}_k$ is then updated to $\boldsymbol{h}_{k+1} = \boldsymbol{h}_k + \boldsymbol{\delta}$. The iteration continues until a prescribed number of iterations is complete or $\|\boldsymbol{\delta}\|$ is smaller than a given tolerance.

C. Obtaining a practically PR BCM filter bank

The error in the PR conditions that is introduced by the linear approximation (38) will vanish as $\|\boldsymbol{\delta}\| \to 0$. This suggests an iterative design method as follows. An SOCP solver is applied to problem (43) with a fixed β and an initial point $\boldsymbol{h}_0$ obtained either by using the algorithm described in Sec. 3 or by (35). To ensure fast convergence, the initial value of β should not be too small. The solution obtained then serves as the initial point for the subsequent iteration where a reduced value of β is adopted. The iteration continues in this way until a solution associated with a sufficiently small β is obtained. Based on (38), we see that the PF so generated practically satisfies the PR constraints while minimizing its stopband energy.

D. Design of OCM filter banks

Like the design algorithm in Sec. 3, the algorithm described above can be readily extended to OCM filter banks with two simple modifications. First, the linear approximation of the PR constraints in this case applies to (17). Consequently, matrix $\boldsymbol{G}_k$ in (39) has a size of $N/4 \times N/2$ whose rows are $\boldsymbol{g}_{ln}^T = 2\boldsymbol{h}_k^T \boldsymbol{Q}_{l,n}^T$ where $\boldsymbol{Q}_{l,n}$ are given by (17b), and vector $\boldsymbol{a}_k$ in (39) has a dimension of $N/4$ whose components are $a_{l,n}(\boldsymbol{h}_k)$ obtained using (17a). In addition, the expression for the stopband energy of the PF in (41) now becomes

$$e(\boldsymbol{h}_k + \boldsymbol{\delta}) = \|2\boldsymbol{P}_L^{1/2}\boldsymbol{V}_e\boldsymbol{\phi} + \tilde{\boldsymbol{b}}_k\| \tag{44}$$

where $\boldsymbol{P}_L$ is given by (37b) and $\tilde{\boldsymbol{b}}_k = 2\boldsymbol{P}_L^{1/2}(\boldsymbol{h}_k + \boldsymbol{\delta}_s)$.

E. Two remarks

We now conclude this section with two remarks.

(1) The algorithmic core of the proposed design methods is SOCP optimization. As a well structured class of convex programming problems, the solution of an SOCP problem is always a global solution which can be identified using an interior-point solver with polynomial-time computational complexity [21]. Having said that, we stress that the design problem itself as formulated in (19) is *not* a convex programming problem because the feasible region defined by the PR constraints is nonconvex, and a solution obtained by the algorithm can only be deemed local. Our approach to the solution may be interpreted as an iterative strategy that allows one to accomplish the design by solving a series of sub-problems that are convex, well-structured, and can be solved efficiently. Although a theoretical proof of the convergence property of the proposed algorithms is presently not available, in quite a number of simulations we had

not detected a single failure of convergence. One might attribute the success of the proposed methods to (i) the global convergence of each SOCP sub-problem, and (ii) the use of constraint (31c) (for the algorithm in Sec. 3) and constraint (43c) (for the algorithm in Sec. 4) that validate the key linear approximations in (25a) and (38), respectively.

(2) The two SOCP-based algorithms proposed in the paper have distinct roles. The first algorithm is aimed at a satisfactory NPR BCM/OCM filter bank. As explained in Figs. 3 and 4, there is a strong likelihood for the algorithm to achieve a globally optimital solution. However, this is accomplished at the cost of reduced design efficiency because the bound β_2 in (31d) can only grow with small increments. As such, the algorithm is only suitable for NPR designs. On the other hand, the second algorithm (in Sec. 4) can accomplish a design significantly more efficiently because it minimizes the stopband energy of the PF directly and allows large increment steps at the beginning of the algorithm. Therefore, it is suitable for the design of practically PR BCM and OCM filter banks. A problem with using a large initial value of β in (42c) is that the "trajectory" of the iterates generated by the algorithm does not offer intermediate results that would correspond to good NPR designs. For these reasons, the two proposed algorithms are considered complementary to each other and should be utilized for different design tasks.

V. EXAMPLES

Example 1: This example is concerned with the design of an NPR OCM filter bank with $M = 32$ and $m = 7$. The length of the linear-phase PF is $N = 448$. The algorithm in Sec. 3 was applied with an initial $\boldsymbol{h}_0$ obtained by minimizing $e_2(\boldsymbol{h},\ w)$ in (34) with $w = 1 - 10^{-9}$, $\omega_p = 0.5\omega_s$, and $\omega_a = 0.9\omega_s$ where ω_s is given by (9c) with $\rho = 1$. The initial values of β_1 and β_2 were set to $\beta_1 = 10^{-3}$ and $\beta_2 = 2 \times 10^{-6}$. The algorithm was implemented using SeDuMi1.05 [33] on a Pentium 4 3.06 GHz PC with MATLAB version 6.5. It took the algorithm 287 iterations (with average CPU time of 0.7104 seconds per iteration) to converge to an NPR OCM filter bank whose performance is illustrated in Fig. 6 and Table I. For comparison purposes, the design is compared to the NPR PCM filter bank presented in [22]. The filter bank also has $M = 32$ channels and the length of the PF is $N = 467$. Its performance is illustrated in Fig. 7 and Table I. As in [22], the total aliasing distortion defined by [8]

$$e_{ta}(\omega) = \left[\sum_{i=1}^{M-1} |T_l(e^{j\omega})|^2\right]^{1/2}$$

was also used in the comparison, see Table I and Figs. 6(d), 7(d). An attractive feature of the method in [22] is that it offers fast design of good NPR OCM filter banks. The present method,

on the other hand, offers still improved designs at the cost of increased amount of computation.

TABLE I

PERFORMANCE COMPARISON OF THE DESIGN IN EXAMPLE 1

	M	N	$e_2(\boldsymbol{h})$	$\max\|e_m(\omega)\|$	$\max\|e_a(\omega)\|$	$\max\|e_{ta}(\omega)\|$
Method of [22]	32	467	$6.95 \cdot 10^{-12}$	$2.42 \cdot 10^{-3}$	$2.67 \cdot 10^{-7}$	$3.86 \cdot 10^{-7}$
Proposed Method	32	448	$4.22 \cdot 10^{-12}$	$1.09 \cdot 10^{-3}$	$1.40 \cdot 10^{-7}$	$1.99 \cdot 10^{-7}$

Example 2: This example is concerned with the design of a practically PR OCM filter bank with $M = 16$, $m = 12$, and $N = 384$. The algorithm in Sec. 4 was applied with initial value of β in (43c) set to 0.001. Two distinct initial $\boldsymbol{h}_0$ were used to test the algorithm's sensitivity to the choice of initial point. The first $\boldsymbol{h}_0$ was obtained by minimizing $e_2(\boldsymbol{h}, w)$ in (34) with $w = 1 - 10^{-9}$, $\omega_p = 0.5\omega_s$, and $\omega_a = 0.9\omega_s$ where ω_s is determined by (9c) with $\rho = 1$. The second $\boldsymbol{h}_0$ was obtained by applying the algorithm in Sec. 3. The performance of the resulting designs turned out to be almost identical, except that the number of iterations when the second $\boldsymbol{h}_0$ was used (147 iterations) was considerably less than that when the first $\boldsymbol{h}_0$ was used (211 iterations). The average CPU time per each iteration was 0.3751 seconds. The performance of the filter bank is evaluated in terms of the amplitude responses of the PF (Fig. 8a), the analysis filters (Fig. 8b), the overall distortion $T_0(e^{j\omega})$, and the alias transfer function $T_l(e^{j\omega})$ for $1 \leq l \leq M - 1$. The PF as well as the analysis (and synthesis) filters have approximately -100 dB stopband attenuation. The reconstruction error was found below -134.80 dB and all amplitude responses of $T_l(e^{j\omega})$ were found below -144.61 dB. An OCM filter bank with the same parameter values $M = 16$ and $m = 12$ was presented in [10] (as Example 2) and its performance was evaluated in Fig. 3 of [10]. By comparison, it is observed that the present design demonstrates improved performance. In addition, the time-domain PR conditions are satisfied with error bound (defined by Eq. (54) in [10]) $\eta \leq 4.34 \times 10^{-19}$ which compares favorably with the bound $\eta \leq 1 \times 10^{-13}$ for the design in [10].

Example 3: This example considers the design of a 16-channel practically PR BCM filter bank with a system delay considerably lower than what an OCM filter bank counterpart can offer. The design parameters are $M = 16$, $m = 3$, $s = 0$, and $d = 31$, which imply $N = 96$ and $D = 31$. The initial point $\boldsymbol{h}_0$ was obtained by minimizing $e_2(\boldsymbol{h}, w)$ in (34) with $w = 1 - 10^{-9}$ and the initial value of β in (43c) was 0.001. The algorithm in Sec. 4 was applied and converged to a solution after 246 iterations with an average CPU time of 0.0627 seconds per iteration.

The stopband energy of the PF was found to be 1.82×10^{-4}, the maximum PR distortion $\max|e_m(\omega)|$, maximum group-delay distortion $\max|e_{gd}(\omega)|$, and maximum worst-case aliasing error $\max|e_a(\omega)|$ were found to be 1.32×10^{-14}, 4.80×10^{-12}, and 1.70×10^{-14}, respectively. The amplitude response of the PF, amplitudes of the analysis filters, amplitude distortion $e_m(\omega)$, group-delay distortion $e_{gd}(\omega)$, and worst-case aliasing error $e_a(\omega)$ are depicted in Fig. 9. Based on above evaluation results, it is evident that the BCM filter bank designed is practically PR. A design of a PR BCM filter bank with $M = 16$, $N = 96$, and $D = 63$ was presented in [23] with its amplitude response of the PF shown in Fig. 5 of [23]. Bearing in mind the present design has the same M and N but a much lower system delay, this example demonstrates the ability of the proposed algorithm to offer satisfactory design of PR BCM filter banks with low system delays.

VI. Conclusions

We have described two SOCP-based algorithms for the design of NPR/PR OCM/BCM filter banks. Although at the moment no theoretical arguments are available to show the global optimality of the designs obtained, computer simulations have demonstrated that the proposed algorithms yield satisfactory NPR and PR designs that are compared favorably with several existing design methods.

Acknowledgment

This work was carried out when the first author was visiting the Tampere International Centre for Signal Processing, Tampere University of Technology, Tampere, Finland. The generous support of the visit from the Centre is greatly acknowledged. The work was also supported by the Academy of Finland, project No. 44876 (Finnish centre of Excellence program (2000–2005)).

References

[1] T. A. Ramstad and J. P. Tanem, "Cosine-modulated analysis-synthesis filterbank with critical sampling and perfect reconstruction," *Proc. IEEE Int. Conf. Acoustics, Speech, and Signal Processing*, vol. 3, pp. 1789-1792, April 1991.

[2] H. S. Malvar, *Signal Processing with Lapped Transforms*, Norwood, MA: Artech House, 1992.

[3] R. D. Koilpillai and P. P. Vaidyanathan, "Cosine-modulated FIR filter banks satisfying perfect reconstruction," *IEEE Trans. Signal Processing*, vol. 40, pp.770-783, April 1992.

[4] H. S. Malvar, "Extended lapped transforms: properties, applications, and fast algorithms," *IEEE Trans. Signal Processing*, vol. 40, pp. 2703-2714, Nov. 1992.

[5] T. Saramäki, "Designing prototype filters for perfect-reconstruction cosine-modulated filter banks," *Proc. IEEE Int. Symp. Circuits Syst.*, vol. 3, pp. 1605-1608, San Diego, CA, May 1992.

[6] T. Q. Nguyen, "A quadratic-constrained least-squares approach to the design of digital filter banks," *Proc. IEEE Int. Symp. Circuits Syst.*, vol. 3, pp. 1344-1347, San Diego, CA, May 1992.

[7] T. Q. Nguyen, "A class of generalized cosine-modulated filter bank," *Proc. IEEE Int. Symp. Circuits Syst*, vol. 2, pp. 943-946, San Diego, May 1992.

[8] P. P. Vaidyanathan, *Multirate Systems and Filter Banks*, Englewood Cliffs, NJ: Prentice Hall, 1993.

[9] N. J. Fliege, "Computational efficiency of Modified DFT polyphase filter banks," *Proc. 27th Asilomar Conf. Signals, Syst., Comput.*, vol. 2, pp. 1296-1300, Pacific Grove, CA, Nov. 1993.

[10] T. Q. Nguyen, "Near-perfect-reconstruction pseudo-QMF banks," *IEEE Trans. Signal Processing*, vol. 42, pp. 65-76, Jan. 1994.

[11] C. D. Creusere and S. K. Mitra, "A simple method for designing high-quality prototype filters for M-band pseudo QMF banks," *IEEE Trans. Signal Processing*, vol. 43, pp. 1005-1007, Apr. 1995.

[12] N. J. Fliege, "Modified DFT polyphase SBC filter banks with almost perfect reconstruction," *Proc. IEEE Int. Conf. Acoustics, Speech, and Signal Processing*, vol. 3, pp. 149-152, Adelaide, Australia, April 1994.

[13] Y.-P. Lin and P. P. Vaidyanathan, "Linear phase cosine modulated maximally decimated filter banks with perfect reconstruction," *IEEE Trans. Signal Processing*, vol. 43, pp. 2525-2539, Nov. 1995.

[14] T. Karp and N. J. Fliege, "MDFT filter banks with perfect reconstruction," *Proc. IEEE Int. Symp. Circuits Syst.*, vol. 1, pp. 744-747, Seattle, WA, May 1995.

[15] T. Q. Nguyen and R. D. Koilpillai, "The theory and design of arbitrary-length cosine-modulated filter banks and wavelets, satisfying perfect reconstruction," *IEEE Trans. Signal Processing*, vol. 44, pp. 473-483, March 1996.

[16] H. Xu, W.-S. Lu, and A. Antoniou, "Efficient iterative design method for cosine-modulated QMF banks," *IEEE Trans. Signal Processing*, vol. 44, pp. 1657-1668, July 1996.

[17] R. A. Gopinath, "Modulated filter banks and wavelets — A general unified theory," *Proc. IEEE Int. Conf. Acoustics, Speech, and Signal Processing*, vol, 3, pp. 1585-1588, Atlanta, GA, May 1996.

[18] G. Schuller and M. J. T. Smith, "New framework for modulated perfect reconstruction filter banks," *IEEE Trans. Signal Processing*, vol. 44, pp. 1941-1954, August 1996.

[19] G. Schuller, "New factorization and structure for cosine modulated filter banks with variable system delay," *Proc. 30th Asilomar Conf. Signals, Systems, and Computers*, vol. 2, pp. 1310-1314, Pacific Grove, CA, Nov. 1996.

[20] T. Q. Nguyen and P. N. Heller, "Biorthogonal cosine-modulated filter banks," *Proc IEEE Conf. Acoustis Speech, and Signal Processing*, vol. 3, pp. 1471-1474, Atlanta, GA, May 1996.

[21] T. Saramäki, "A generalized class of cosine-modulated filter banks," *Proc. First Int. Workshop on Transforms and Filter Banks*, pp. 336-365, Tampere, Finland, Feb. 1998.

[22] Y.-P. Lin and P. P. Vaidyanathan, "A Kaiser window approach for the design of prototype filters of cosine modulated filterbanks," *IEEE Signal Processing Letters*, vol. 5, pp. 132-134, June 1998.

[23] P. N. Heller, T. Karp, and T. Q. Nguyen, "A general formulation of modulated filter banks," *IEEE Trans. Signal Processing*, vol. 47, pp. 986-1002, April 1999.

[24] G. Schuller and T. Karp, “Modulated filter banks with arbitrary system delay: Efficient implementations and the time-varying case,” *IEEE Trans. Signal Processing*, vol. 48, pp. 734-748, March 2000.

[25] T. Karp, A. Mertins, and G. Schuller, ‘Efficient biorthogonal cosine-modulated filter banks,” *Signal Processing*, vol. 81, pp. 997-1016, May 2001.

[26] T. Saramäki and R. Bregović, *Multirate Systems and Filter Banks*, Chapter 2 in Multirate Systems: Design and Applications, ed. by G. Jovanovic-Dolecek, Hershey PA: Idea Group Publishing, 2002.

[27] R. Bregović and T. Saramäki, “A systematic technique for designing prototype filters for perfect reconstruction cosine modulated and modified DFT filter banks,” *Proc. IEEE Int. Symp. Circuits Syst.*, vol. 2, p. 33-36, Sydney, Australia, May 2001.

[28] R. Bregović and T. Saramäki, “An efficient approach for designing nearly perfect-reconstruction low-delay cosine-modulated filter banks,” *Proc. IEEE Int. Symp. Circuits Syst.*, vol. 1, pp. 825-828, Scottsdale, AZ, May 2002.

[29] K. Schittkowski, “NLPQL: A FORTRAN subroutine solving constrained nonlinear programming problems,” Ann. Oper. Res., vol. 5, pp. 485-500, 1986.

[30] M. S. Lobo, L. Vandenberghe, S. Boyd, and H. Lebret, “Applications of second-order cone programming,” *Linear Algebra and Applications*, vol. 248, pp. 193-228, Nov. 1998.

[31] A. Ben-Tal and A. Nemirovski, *Lectures on Modern Convex Optimization*, SIAM, Philadelphia, 2001.

[32] F. Alizadeh and D. Goldfarb, “Second-order cone programming,” *Rutcor Research Report* 51-2001, Rutgers Center for Operations Research, Rutgers University, Piscataway, NJ, Nov. 2001.

[33] J. F. Sturm, “using SeDuMi 1.02, a MATLAB toolbox for optimization over symmetric cones,” *Optimization Methods and Software*, vol. 11-12, pp. 625-653, 1999.

[34] R. H. Tütüncü, K. C. Toh, and M. J. Tood, “SDPT3 — A MATLAB software package for semidefinite-quadratic-linear programming”, version 3.0, August 2001.

[35] L. Vandenberghe and S. Boyd, “Semidefinite programming,” *SIAM Review*, vol. 38, pp. 49-95, March 1996.

[36] P. Gahinet, A. Nemirovski, A. J. Laub, and M. Chilali, *Manual of LMI Control Toolbox*, The MathWorks Inc., Natick, MA, 1995.

[37] G. H. Golub and C. F. Van Loan, *Matrix Computations*, 3rd ed., The Johns Hopkins University Press, 1996.

[38] D. G. Luenberger, *Linear and Nonlinear Programming*, 2nd ed., Addison-Wesley, 1984.

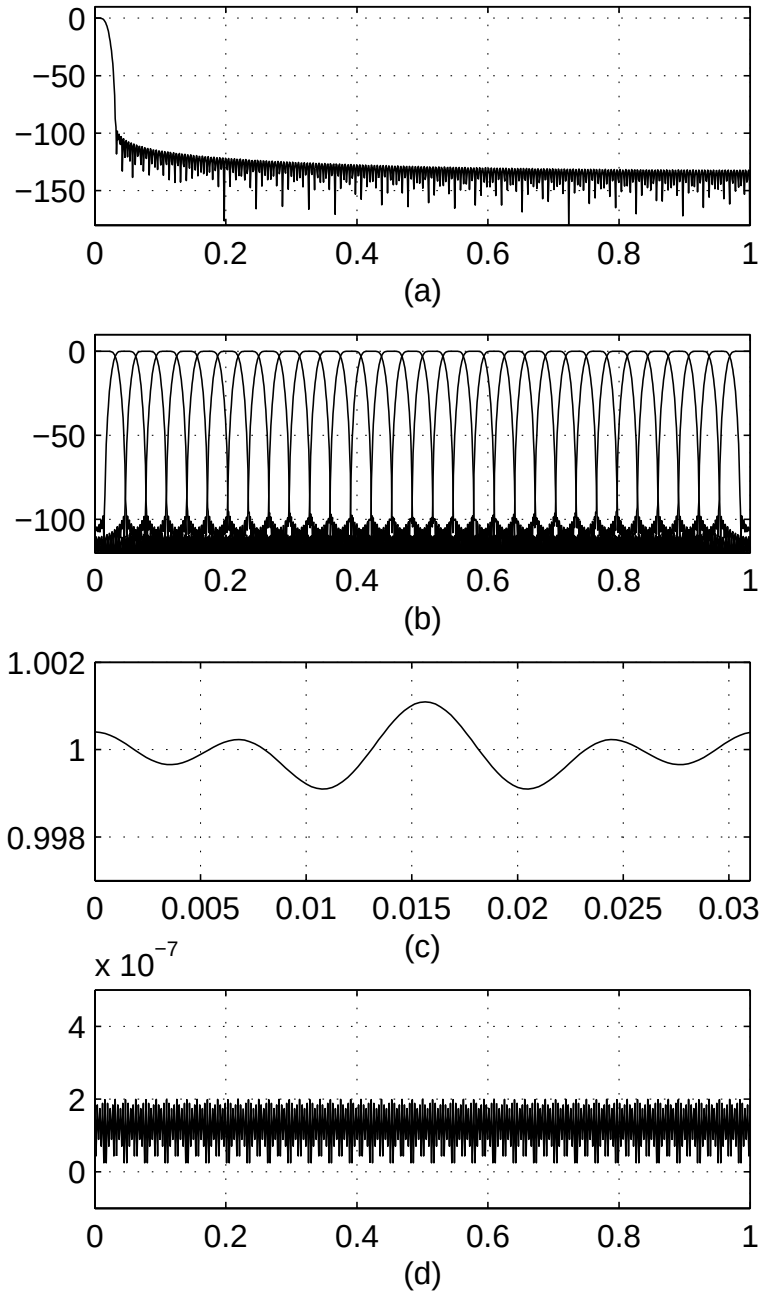

Fig. 6. A 32-channel NPR OCM filter bank with $N = 448$. (a) Amplitude responses of the PF. (b) Amplitude responses of analysis filters. (c) Amplitude of $T_0(e^{j\omega})$ on $[0,\ \pi/M]$. (d) Total aliasing error $e_{ta}(\omega)$.

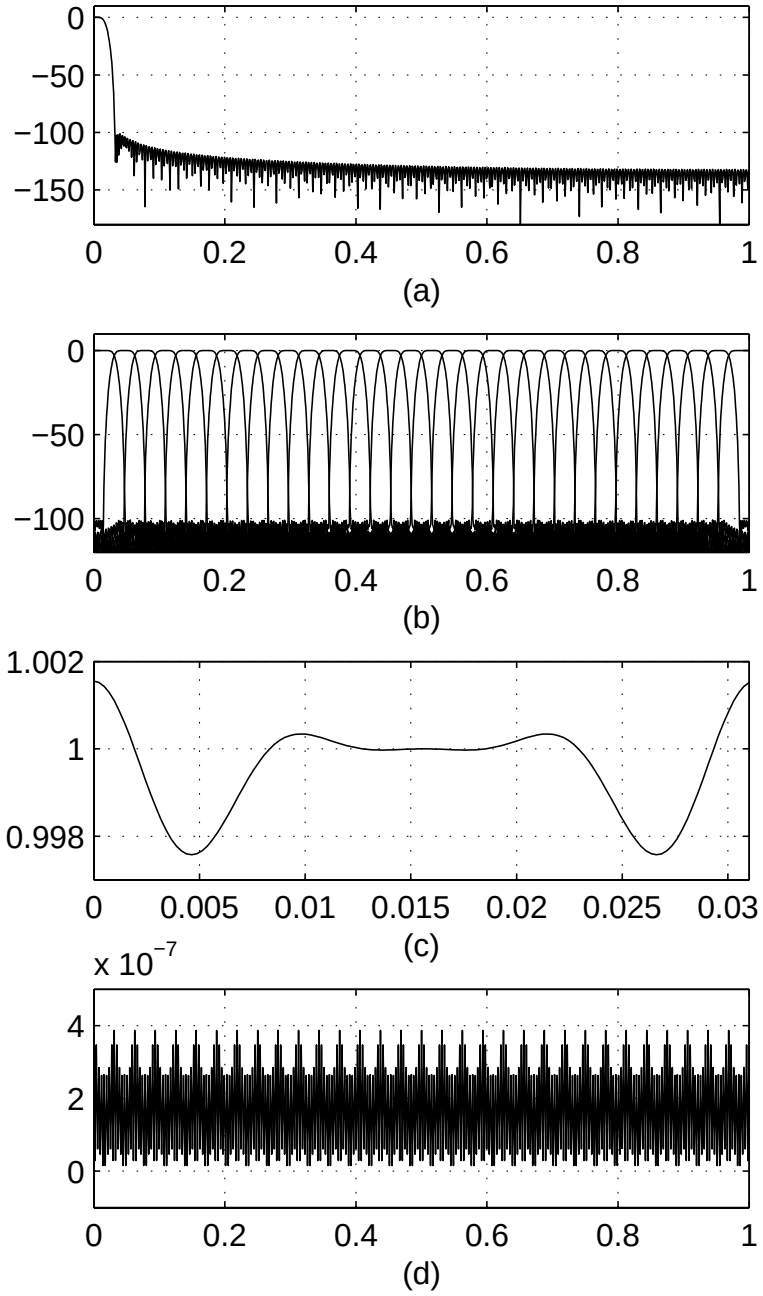

Fig. 7. A 32-channel NPR OCM filter bank with $N = 467$ presented in [22]. (a) Amplitude responses of the PF. (b) Amplitude responses of analysis filters. (c) Amplitude of $T_0(e^{j\omega})$ on $[0,\ \pi/M]$. (d) Total aliasing error $e_{ta}(\omega)$.

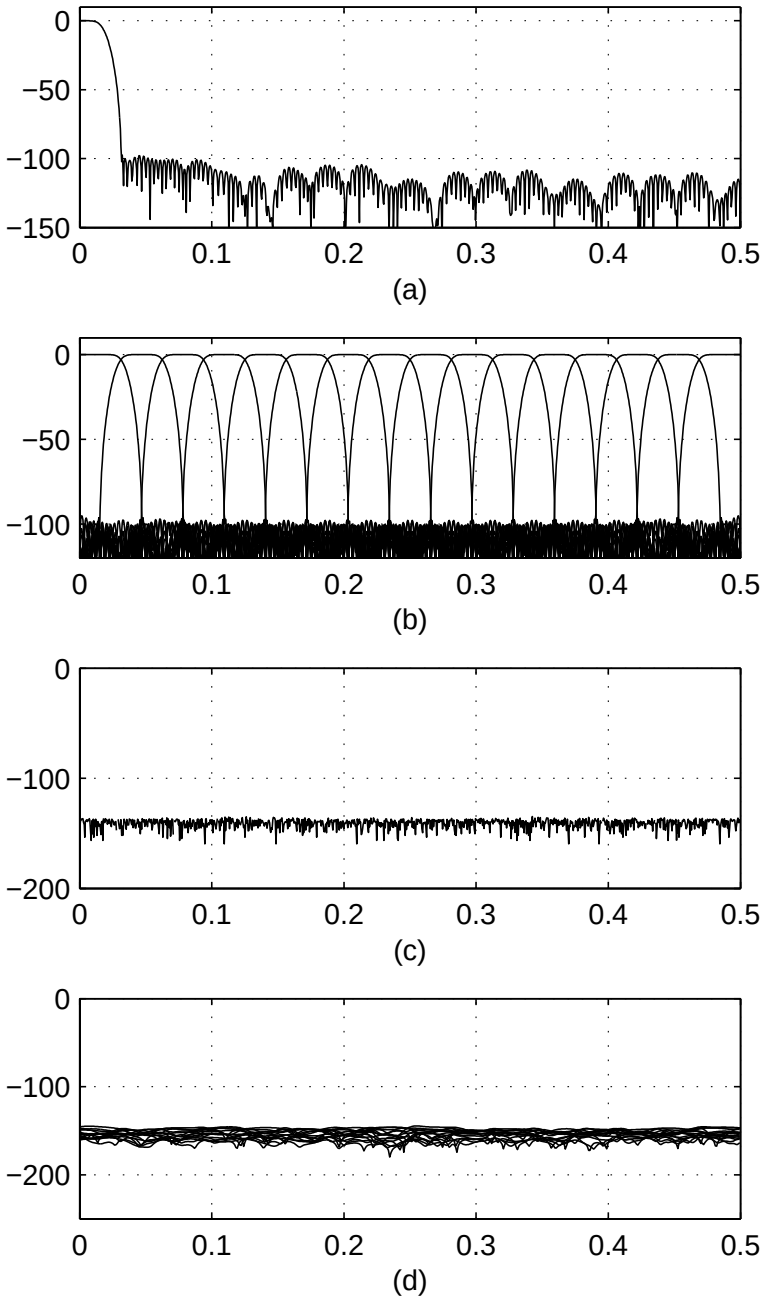

Fig. 8. A 16-channel PR OCM filter bank with $N = 384$. (a) Amplitude response of the PF. (b) Amplitude responses of the analysis filters. (c) Reconstruction error in dB. (d) Amplitude responses of the alias transfer functions $T_l(z)$ for $1 \leq l \leq 15$.

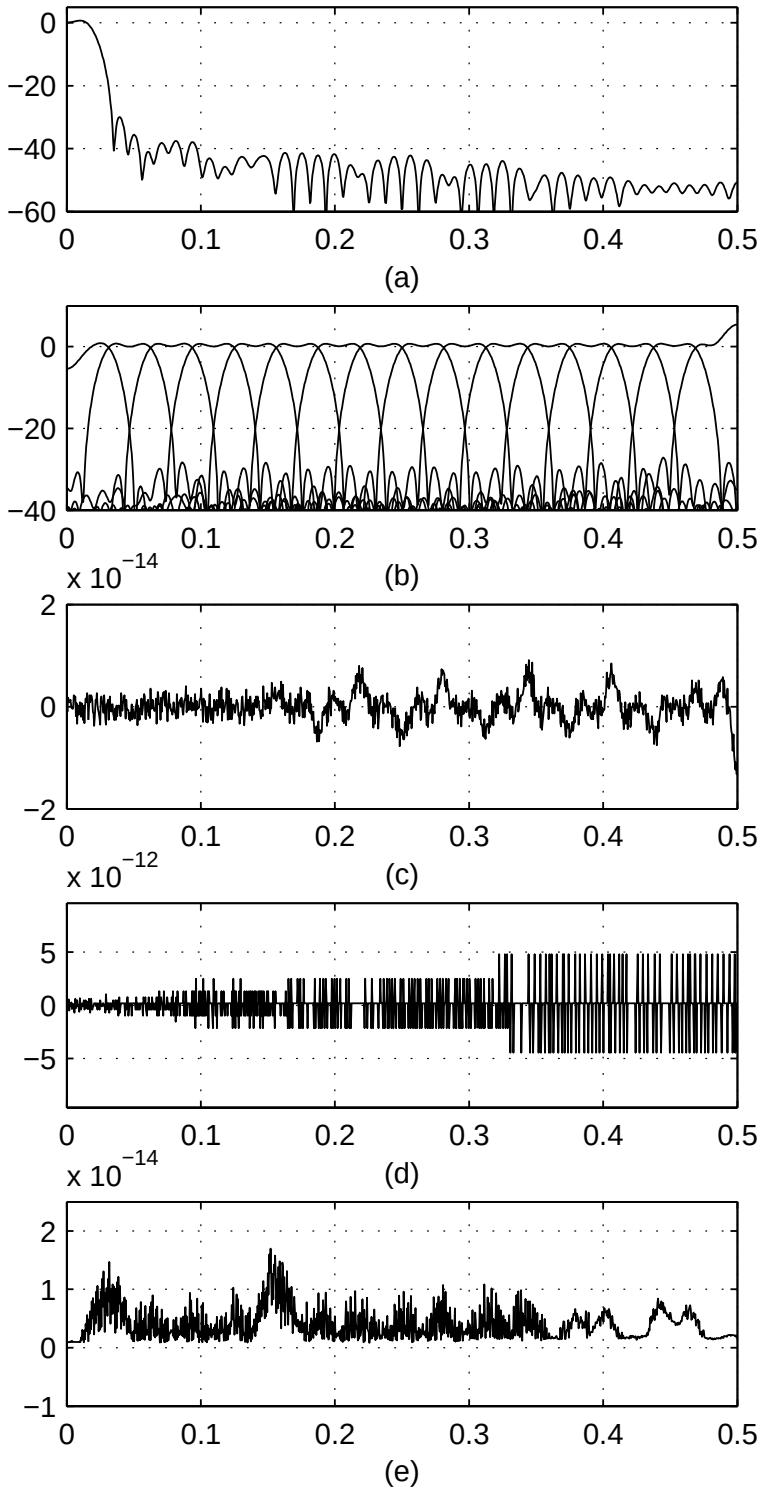

Fig. 9. A 16-channel PR BCM filter bank with $N = 96$ and $D = 31$. (a) Amplitude response of the PF. (b) Amplitude responses of the analysis filters. (c) Amplitude distortion. (d) Group-delay distortion. (e) Worst-case aliasing error.